Formation of localized hole states in complex oxides: I. Hole states in $BaTiO_3$

1997 J. Phys.: Condens. Matter 9 6359

(http://iopscience.iop.org/0953-8984/9/30/005)

J. Phys.: Condens. Matter **9** (1997) 6359–6370. Printed in the UK PII: S0953-8984(97)80351-7

Formation of localized hole states in complex oxides: I. Hole states in $BaTiO_3$

H Donnerberg, S Többen and A Birkholz
University of Osnabrück, FB Physik, D-49069 Osnabrück, Germany

Received 16 December 1996, in final form 21 April 1997

Abstract. Defect electrons (holes) play an important role in most technologically important complex oxides. In this contribution we present the first detailed characterization of localized hole states in such materials. Our investigations employ advanced embedded-cluster calculations which consistently include electron correlations and defect-induced lattice relaxations. This is necessary in order to account for the variety of possible hole-state manifestations. Even in highly ionic oxides such as MgO, there exists a delicate interplay between electron correlations and defect-induced lattice deformations.

1. Introduction

The basic structural building units of solid oxides are MO_6 metal–oxygen octahedra, and, possibly, additional MO_4 tetrahedra. The complete crystal structure is built up of corner-, face-, and/or edge-sharing connections of these structural elements. Additional cations (A) can be incorporated at interstitial lattice sites. These are increasingly formed, the more open structured the whole network of MO_n units appears to be. Generally, open crystal structures imply high formal M-cation charge states (referring to formal O^{2-} anions) leading to mixed ionic–covalent (or semi-ionic) material properties. The M cations are in most cases transition-metal (TM) ions. Examples of such complex materials are given by AMO_3 perovskite-structured oxides such as barium titanate ($BaTiO_3$). Perovskite oxides are frequently ferroelectric, and have important electro-optic applications based on the photorefractive effect. Also the structure of high-T_c oxides resembles the perovskite structure.

Charge carriers, either valence-band (VB) holes or conduction-band (CB) electrons, are created by doping with impurities, annealing treatments, or by light-induced charge-transfer excitations which, for example, take place during photorefractive processes in the appropriate oxides. Combined optical absorption and electron spin-resonance measurements (photo-ESR) [1] proved that the created and subsequently trapped holes influence the light-induced charge-transfer reactions in photorefractive $BaTiO_3$. These holes, which are either paramagnetic or diamagnetic, probably induce the observed sublinear dependence of the photoconductivity on the light intensity (see, e.g., [2]). A further example highlighting the relevance of holes refers to high-T_c oxides: pairs of doped holes give rise to superconductivity in these materials. The possible pairing scenarios are still a matter of active debate.

The present work initiates a systematic and detailed characterization of localized hole states in complex oxides. Our investigations employ real-space embedded-cluster

0953-8984/97/306359+12$19.50

calculations, which consistently combine electron correlations and defect-induced lattice relaxations. This procedure is indispensable in order to predict the richness of possible hole states. Here, we demonstrate simulations for trapped holes in $BaTiO_3$, but many results, ranging from the stabilization of cationic charge states to the formation of bipolarons, can be extrapolated to other oxides.

The trapping of holes at acceptor defects leads to a localization of hole states, which is further aided by defect-induced lattice distortions. In near-insulating high-T_c oxides, the antiferromagnetic order supports hole localizations. Principally, there is 'on-acceptor' and 'off-acceptor' hole trapping. In the first case the trapped hole localizes at the acceptor site (thereby increasing the acceptor charge state by one positive unit, i.e. $M^{+n} + h^{\bullet} \longrightarrow M^{+(n+1)}$), and in the second case the hole remains sited at the oxygen ligands. Further, the off-acceptor case allows one to classify hole states according to their degree of delocalization, i.e. complete localization at exactly one ligand anion, intermediate localization at two neighbouring oxygen ions (V_K centres), and delocalization over more than two oxygen ligands.

Which hole-localization type is favoured depends on the ionicity of the host system, but also on the incorporation site and electronic structure of the acceptor. For example, at Ba-site acceptors, localized off-acceptor holes are likely to be preferred over delocalized species due to large interionic separations [3]. Further, the simultaneous binding of two holes at one acceptor facilitates the formation of small intersite bipolarons representing negative-U centres. Such species could explain the diamagnetic hole centres in photorefractive oxides [1]; intersite bipolarons have also been considered as possible superconductivity-carrying bosons in high-T_c oxides (see [4], for details). Earlier work on bipolarons in oxide materials dealt exclusively with electron-type species. We quote in this context the pioneering work of P W Anderson [5] on the formation of negative-U centres in amorphous solids. Schlenker [6] investigated small electron-type bipolarons in titanium oxides.

2. Methods

Our investigations employ real-space embedded-cluster calculations (ECC), in which the crystal is divided into (i) a central and quantum-chemically treated defect cluster, and (ii) the embedding lattice, which is modelled more approximately. The ECC discussed in this article deal with the trapping of holes at Ti-site acceptors in $BaTiO_3$. Our calculations are based on 21-atom clusters, $MO_6Ba_8Ti_6$, centred around an acceptor–oxygen octahedron MO_6; see also [7]. All of the simulations assume the perfect-crystal structure of cubic $BaTiO_3$. This simplification may be justified due to the observation that all possible ferroelectric distortions of the material are small compared with usual defect-induced lattice relaxations.

The molecular orbital *ansatz* for the central MO_6 complex employs Gaussian-type basis functions with a split-valence quality for the acceptor metal impurity and its oxygen ligands; the oxygen basis set is further augmented with polarizing d functions. Bare effective core potentials [8] are used to model the localizing ion-size effects of the outer Ba and Ti cations. The *ab initio* level of our calculations covers Hartree–Fock (HF) theory, Møller–Plesset perturbation theory to second order (MP2) and density functional theory (DFT). All quantum cluster simulations have been performed on the basis of the quantum-chemical CADPAC code [9]. Within DFT two choices are used to approximate the exchange–correlation functional, i.e. the local spin-density *ansatz* of Vosko, Wilk and Nusair [10] (VWN-LSDA) and the generalized-gradient approximation functional involving the Becke exchange term [11] and the correlation functional derived by Lee, Yang and Parr [12]. This functional, abbreviated as 'BLYP', improves on the LDA.

The modelling of the embedding lattice and of cluster–lattice interactions employs a shell-model pair-potential description (see also references [7, 13, 14]). The shell-model parameters have been taken from the earlier work of Lewis and Catlow [15]. It is noted that the shell model takes electronic polarization contributions of the embedding lattice ions reasonably well into account. This feature is particularly important as regards the highly polarizable oxygen anions. Figure 1 displays the embedding scheme.

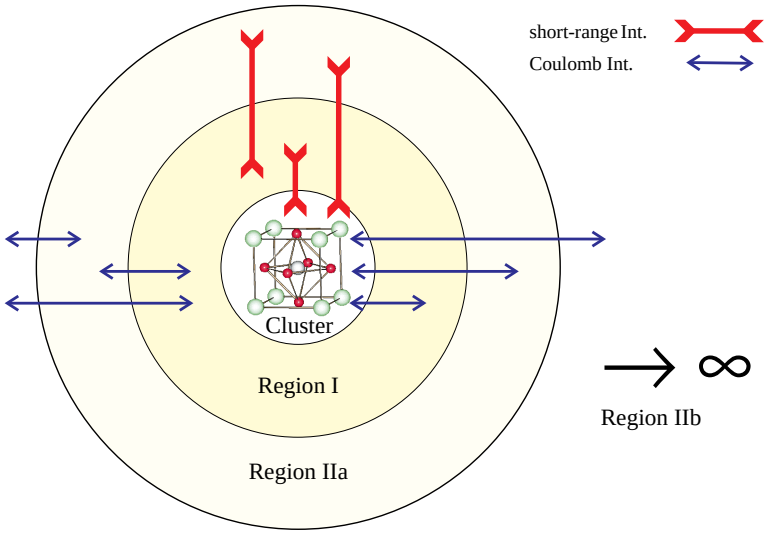

Figure 1. A schematic diagram of the embedded-cluster calculations. The quantum cluster is embedded in a classically treated lattice consisting of the regions I, IIa, and IIb. The arrows indicate the various interactions between the crystal regions.

As in any classical Mott–Littleton defect calculation, the (embedding) crystal lattice is divided into three regions: region I which is explicitly equilibrated according to the underlying pair potentials, the interface region IIa, and region IIb. Region II (a and b) is treated as a polarizable continuum using the harmonic approximation for the region-II self-energy. Whereas the interactions between the cluster and region I, on the one hand, and region IIa, on the other hand, are included explicitly, all region-IIb species feel only the effective defect charge of the central defect cluster. Details of this well-known description are given in reference [16]. All of the lattice calculations employ the CASCADE code [17].

The total energy of the complete model crystal is given by the expression

$$E(\rho, R_c, R_r) = \min_{\rho, R_c, R_r} \{E^{\mathrm{QM}}_{\mathrm{Clust}}(\rho, R_c) + E^{\mathrm{SM}}_{\mathrm{Env}}(R_r) + E^{\mathrm{Int}}(\rho, R_c, R_r)\}. \qquad (1)$$

ρ, R_c, and R_r denote the cluster electron density, the coordinates of the cluster nuclei, and the positions of the shell-model species in the embedding environment, respectively. $E^{\mathrm{QM}}_{\mathrm{Clust}}$ represents the quantum-mechanically calculated cluster self-energy, $E^{\mathrm{SM}}_{\mathrm{Env}}$ the Mott–Littleton-type shell-model energy of the embedding environment, and E^{Int} is the cluster–lattice interaction energy. The required minimization in equation (1) is performed using the programs CADPAC (variation of ρ with fixed R_r) and CASCADE (variation of R_r with fixed R_c and ρ). In order to perform cluster geometry optimizations which are consistent with a predetermined embedding crystal lattice (represented by a point-charge field), an additional program has been written which updates the total cluster energies and gradients, as calculated by any quantum-chemical program such as CADPAC, by adding the appropriate

short-range pair-potential contributions due to the interactions between cluster ions and embedding lattice species. With these updates, the program carries through the cluster geometry optimization using a variable-metric (quasi-Newton) minimization algorithm. The total minimization procedure is completed when the main cycle consisting of the alternating lattice- and cluster-equilibration subcycles converges. It is finally noted that we have neglected the full cluster multipole consistency during the embedding-lattice relaxation step (see [18] for details), since, in our simulations, we did not observe any appreciable relaxation and energy changes due to cluster multipole contributions deviating from formal-charge models.

Before proceeding to the results obtained, we briefly discuss the merits and possible shortcomings of the present embedded-cluster approach. Our methodology proves to be the only successful one which can consistently integrate the local electronic structure and large-scale lattice-distortion effects. In particular, we find the combination of DFT and of our embedding scheme to be sufficiently accurate and flexible to realistically account for the variety of possible hole states. We stress that cutting off the electronic structure beyond the cluster boundary does not in principle invalidate our results. This is due to the fact that embedded-cluster calculations formally refer to a localized-orbital point of view (e.g. see [19, 7] for related discussions), and not to the extended one-electron eigenstates of the crystal. Generally, the two orbital descriptions are unitarily equivalent. Moreover, for insulating materials this statement also holds true when restricting the domain of definition of the unitary transformation to the subsets of occupied orbitals [20]; thus, the crystalline electron density can be represented either by occupied Bloch states or by an equal number of occupied localized orbitals. This statement, which ultimately justifies embedded-cluster calculations in properly chosen systems, is not true for metals. But even for suitable materials it is important to specify accurate localizing potentials in order to derive appropriate localized orbitals. This has been discussed to some extent in references [19, 21]. In approximating the exact localizing potentials we previously used bare effective core pseudopotentials, which were implemented at the boundary cations of the quantum cluster [7], and obtained very satisfactory results. At first glance the use of bare pseudopotentials seems to be questionable, since this approximation neglects any existing covalent charge transfer directed from the cluster oxygen anions onto the boundary titanium cations. However, the perfect-crystal simulations considered in reference [7] prove the reliability of this approximation. Simulations of this type are able to provide information on the quality of the particular embedded-cluster approach chosen. The calculated ion displacements due to cluster–lattice mismatch turned out to be less than 3% of the lattice constant. Further, preliminary tests including the valence orbital structure of the boundary Ti cations indicate no qualitative changes regarding the localization properties of trapped holes. Since these extended calculations become very expensive computationally, we restricted further simulations to the bare-ECP approximation.

In the case of defect simulations, the cluster should be chosen large enough to contain all relevant parts of the defect wave function. This requirement is expected to be fulfilled in our simulations of trapped holes: all of the hole states considered in this contribution can be assumed to be essentially localized within the cluster region due to the presence of the hole–attractive-acceptor defect and due to pronounced lattice deformations (the small-polaron effect). Defect-induced electronic redistributions of the cluster environment are expected to be accounted for within the shell-model lattice polarizability employed. Further indications of the reliability of our present results are provided by our earlier calculations of optical charge-transfer (CT) transitions at transition-metal cations [7], which compare

favourably with experimental data. The CT states may be considered as excited states of trapped holes.

Next we mention the neglect of the full cluster multipole consistency. The implications of this simplification might have been crucial, if we had considered bare MO_6 clusters. But due to the pseudopotential Ba and Ti cations at the cluster boundary, not only have ion-size effects been modelled, but also the effective separation between the embedding lattice and the MO_6 electron density has been increased significantly. Thus, higher-multipole contributions, which fall off rapidly with increasing distance, are much less important in the embedding lattice region. Indeed, for the JT-active Fe_{Ti}^{4+} defect having non-vanishing quadrupole moments, the total energy differences (including lattice relaxations) between formal-charge and multipole-consistent models turned out to be less than 0.01 eV. For off-acceptor hole states (e.g. the Al_{Ti}^{3+}–V_K centre; see section 3) we observed corresponding energy differences of about 0.1 eV, which in most instances do not appreciably influence any conclusions drawn. We note that this difference increases into the 1 eV range, if one omits the inclusion of ECP-boundary cations.

Finally, we consider the implications of our chosen correlation levels. We have used MP2, known to be size consistent, and DFT. MP2, the lowest order of many-body perturbation theory, provides lower bounds to the absolute correlation energy. The inclusion of higher orders would be impractical even for our MO_6 subclusters. Many of the subsequent calculations have been performed with DFT, too. As mentioned above, we used the spin-polarized LDA as well as the GGA functional BLYP. L(S)DA is known to grossly overestimate correlation contributions (and thus molecular binding energies), but this deficiency is removed to a considerable extent upon using BLYP. For example, calculations on simple dimer molecules (e.g. F_2) confirm that MP2 provides lower bounds to the molecular binding energy, and BLYP, in turn, provides upper bounds: -1.4 eV (MP2), -1.7 eV (exact, [22]) and -2.2 eV (BLYP). In contrast, LSDA considerably overestimates the molecular binding energy; for example, the fluorine binding energy becomes -3.4 eV within the VWN-LSDA approximation. The same behaviour is found for peroxide bipolarons (see section 3). In general we can assume that the exact results (within the limitations of the present model) are reasonably bounded by the MP2 and DFT-BLYP approaches towards electron correlation. Whereas MP2 typically underestimates electronic correlations by 10–20% [23], DFT-BLYP overestimates the same effects by only 5–10%, with almost exact reproductions of the exchange contributions achieved at the same time. This result, which demonstrates the very satisfactory quality of DFT-BLYP exchange–correlation energies, can be inferred from a recent comparison of different DFT exchange–correlation energies with exact results for a number of ions [24]. This review also shows that L(S)DA often produces correlation energies exceeding exact values by some hundred per cent. The high quality of DFT-BLYP can also be assessed from recently calculated molecular binding energies [25]; again, within 5–10% these data fit with the corresponding exact energies. Thus, as a probably reliable estimate of the exact correlation energy, one may take the average of the MP2 and DFT-BLYP results.

We have also performed preliminary simulations regarding the localization of holes trapped at Li acceptors in magnesium oxide. For these centres the formation of delocalized off-acceptor holes is unlikely (see also references [26, 27] for related theoretical discussions), and it appears to be reasonable to test this expectation taking account of electron correlations as discussed above. Noticeably, all previous simulation studies have been essentially confined to HF-type calculations. Magnesium oxide having the close-packed NaCl structure behaves almost perfectly ionically. The results of these simulations will be discussed in the following section, too.

3. Results and discussion

In the following discussion, in each case we start with the ionic HF model, and add on correlations afterwards to demonstrate important implications.

Table 1. Total HF and MP2 embedded-cluster energies for different hole states, including lattice relaxations. Energies are renormalized to localized off-acceptor states. $O_O^-(\pi,\sigma)$: localized off-acceptor holes in oxygen 2p π- or σ-type orbitals. $(O(xy))^-$: off-acceptor holes delocalized over the four oxygen ligands in the xy-plane. $2S+1$ denotes the total spin multiplicity of the cluster. Note that Fe^{3+} and Cr^{3+} favour high spin ($2S_{Fe}+1=6$, $2S_{Cr}+1=4$), and Rh^{4+} favours low spin ($2S_{Rh}+1=2$).

Defect	$2S+1$	ΔE_{total}^{UHF} (eV)	ΔE_{total}^{MP2} (eV)
Fe_{Ti}^{3+}–$O_O^-(\pi)$	7	0.0	0.0
Fe_{Ti}^{3+}–$O_O^-(\pi)$	5	0.0	—
Fe_{Ti}^{3+}–$O_O^-(\sigma)$	7	+1.1	—
Fe_{Ti}^{3+}–$O_O^-(\sigma)$	5	+1.0	—
Fe_{Ti}^{3+}–$(O(xy))^-$	7	+2.4	+0.5
Fe_{Ti}^{4+}	5	+2.4	+0.1
Rh_{Ti}^{3+}–$O_O^-(\pi)$	2	0.0	0.0
Rh_{Ti}^{3+}–$(O(xy))^-$	2	+2.7	+0.1
Rh_{Ti}^{4+}	2	+0.4	−2.4
Cr_{Ti}^{3+}–$O_O^-(\pi)$	5	0.0	0.0
Cr_{Ti}^{4+}	2	+1.15	−2.6

First, we discuss single holes trapped at TM cations. Within HF theory, on-acceptor holes are favourable for divalent TM cations including Cu^{2+}, which possess filled electron levels above the VB edge. At trivalent Ti-site TM acceptors, on the other hand, localized (i.e. symmetry-breaking) off-acceptor holes are highly preferred (table 1). Here, we observe the hole localization in π-type oxygen 2p orbitals (perpendicular to the oxygen–acceptor axis). This symmetry-broken state is stabilized by defect-induced lattice distortions, and, in this way, it can acquire physical significance. The relaxation-induced energy gain is typically 1 eV, which emphasizes the importance of such terms. The occurrence of symmetry-broken solutions may be considered as electronic polaron self-trapping. Generally, hole localization in σ-type orbitals (parallel to the oxygen–acceptor axis) is less favourable, but deviations may occur due to the actual electronic acceptor structure or due to the nature of the particular host oxide (see below).

Interestingly, both delocalized off-acceptor holes and the formation of tetravalent TM ions are unfavourable within HF theory. For example, delocalized off-acceptor holes are separated by 2–3 eV from their localized counterparts. Similar results have been obtained in previous HF simulations on trapped single holes in MgO [26, 27] and NiO [28]. Also, these calculations predict localized off-acceptor holes to be the most favourable. In fact such holes are likely to represent the most favourable off-acceptor solutions for highly ionic oxides such as MgO, but this behaviour will certainly prevail in any HF calculation, thus simulating artificially strong ionic situations. In this context we briefly consider our preliminary simulations on holes in MgO trapped at Li acceptors; a detailed discussion of this will be deferred to a forthcoming publication. The particular quantum cluster corresponding

to the formula LiO_6Mg_{18} has been chosen. All Mg cations have been modelled using bare effective core potentials [8], whereas the quality of the Gaussian basis set of the central LiO_6 complex corresponds to that of $BaTiO_3$. We included cluster geometry optimizations (i.e. short-range lattice deformations) but neglected the relaxation of the embedding lattice (i.e. long-range lattice distortions) at this preliminary stage.

Our HF simulations unambiguously suggest that the localized off-acceptor hole state is the ground state. Within these calculations the localized state is 3.8 eV more favourable than the completely delocalized off-acceptor state, with the hole distribution equally divided among all six oxygen ligands. The present HF energy difference is modestly larger than a previously reported value of 3 eV [28], which refers to calculations on a small LiO_6 cluster embedded in an array of point charges representing the relaxed lattice environment of NiO (within this model NiO and MgO are almost identical). Thus, ion-size effects were not included in these earlier simulations; however, they would have been important, due to the dense packing of these materials. We believe that the energetical deviation encountered above may be ascribed essentially to the additional ion-size effects due to cations next to the LiO_6 cluster, which have been considered in our present simulations. It is noted further that, unlike the case for $BaTiO_3$, trapped holes in MgO prefer to occupy σ-type oxygen 2p orbitals. This is consistently seen from all HF and DFT calculations performed, and refers to the strong neighbour-cation influences, too. We would like to stress that another hole state deserves particular attention. This state, which has been discussed as an alternative to the completely localized (one-centre) hole state [29, 26], corresponds to a linear two-centre hole distribution over two adjacent oxygen ligands, i.e. to $O^{-1.5}$–Li^{+}–$O^{-1.5}$. Again, the hole localizes in σ-type 2p orbitals, which ideally fits with this two-centre hole distribution. The energy difference from the completely localized hole state amounts to 1.9 eV (2.2 eV according to previous INDO simulations [26]). This state is not affected by disturbing cation-size effects.

Ion-size effects also influence the results of correlated calculations for rock-salt-structured binary oxides. Our DFT simulations of delocalized hole states, which enforce the full cubic symmetry, show that a complete hole delocalization is unfavourable due to the ion-size effects discussed above. Correlation contributions are significantly more effective in the case of hole states where this interaction is small. Corresponding states refer to the completely localized hole and to the linear hole distribution over two adjacent oxygen ligands. Our preliminary simulations suggest that the latter state becomes the ground state upon inclusion of correlations and neglecting long-range lattice deformations at the same time. In this approximation the two-centre state is significantly more favourable, by 1.6 eV (DFT-BLYP), than the one-centre localized hole state. Within the minimal-correlation MP2 approximation we find only a marginal preference for the completely localized hole state (magnitude: 0.3 eV) over the $O^{-1.5}$–Li^{+}–$O^{-1.5}$ distribution. Basis-set dependences of these calculations have been tested by adding further polarizing oxygen d functions and by breaking down the oxygen 2p contractions into primitives, but these modifications did not affect the results. Therefore, the deviations will essentially refer to the different degrees of correlation accounted for within the MP2 and DFT-BLYP methods. Considering the average correlation-energy difference leads to the suggestion that the two-centre hole state represents the ground state. We recall that this average value is expected to provide reliable estimates of correlation contributions. Consequently, long-range lattice deformations that have been neglected so far will ultimately be decisive as regards the nature of the trapped-hole ground state. In fact, such terms are the more effective the more localized the state considered is. Shell-model estimates suggest that a corresponding relaxation-energy difference ranges between some tenths of an eV and $\simeq$1 eV in favour of the one-centre hole, but, in any case,

this additional energy contribution leaves both hole states highly competitive with each other. Additional detailed work is in progress to finally resolve the ground-state question.

In summary, it seems that the space-filling crystal structure of MgO (and, similarly, that of NiO), which results from the ionic bonding properties of the materials, impedes the formation of completely delocalized hole states. However, we may conclude that even in correspondingly ionic materials there exists a delicate balance between electronic structure effects and lattice-distortion effects, identifying one-centre or two-centre hole distributions as the proper ground states. In any case, the situation in favour of one of these hole states is much less clear than is indicated by the simulation based on HF-based calculations.

The situation becomes different to some extent in complex semi-ionic oxides such as $BaTiO_3$, where the MO_6 bonding units are increasingly isolated due to the less dense packing. In the case of off-acceptor hole states, this marked difference between ionic close-packed binary oxides and complex oxides favours the occupation of π-type oxygen orbitals, and can, in principle, further increase the hole-delocalization properties. This will be seen below. Therefore, the hole-localization properties can show a broad range of modifications in the more complex materials.

In $BaTiO_3$ the effects of electron correlation are most significant for trivalent TM acceptors, due to the increased covalent charge transfer from oxygen onto the TM ions. This has important consequences: the on-acceptor hole localization is enhanced, and, simultaneously, possible off-acceptor holes increasingly delocalize. In contrast, TM cations that are at most divalent, including Cu^{2+} on-acceptor holes, remain stable. This behaviour differs from that of La_2CuO_4, for which, as confirmed by our preliminary ECC, doped holes localize at the oxygen sites. The different *effective* copper charges in the two oxides can explain such deviations. Further work on La_2CuO_4 is in progress.

Our MP2 calculations (table 1) illustrate that electron correlation tends to favour on-acceptor holes at trivalent TM acceptors. Rh^{4+} and Cr^{4+} become preferred over $M–O^-$ centres, but Fe^{4+} remains 0.1 eV less favourable than $Fe^{3+}–O^-$. Within DFT, even Fe^{4+} is stable, which agrees with experimental experience, and for all trivalent TM acceptors the most favourable off-acceptor holes are delocalized at this level.

Considering off-acceptor holes, correlation mostly affects the delocalized hole states, but also affects localized states to a much lesser extent. These off-acceptor-hole results demonstrate the pronounced interplay between orbital relaxations and electron correlation, i.e. the localized hole states with significant HF orbital relaxations receive less correlation-energy gain than delocalized hole states. However, unlike in HF theory, the energy separations between localized and delocalized off-acceptor holes remain within some tenths of an eV. This result indicates that a modest increase of ionicity could favour localized off-acceptor holes over delocalized ones. The lanthanide contraction of 5d TM cations might accomplish such changes, leading to observable localized off-acceptor holes, if these are sufficiently stable against the formation of on-acceptor holes. ESR data suggest that localized off-acceptor holes bound to ESR-silent Pt acceptors exist in $BaTiO_3$ [3]. The charge state of platinum could not be assessed experimentally, but Pt^{4+} with a completely filled $5d(t_{2g})$ subshell is a possible candidate.

In summary, electron correlation essentially stabilizes the high-valency charge states of various TM cations in $BaTiO_3$. This mechanism resembles the Haldane–Anderson scenario [30] for semiconductors. For highly ionic materials, in contrast, the charge-state stabilization has been ascribed to lattice relaxations [31]. The present discussion confirms that $BaTiO_3$ is semi-ionic.

In comparison to those of most TM acceptors, the hole-localization properties can differ at ionic acceptor cations due to the lack of filled acceptor levels above the VB edge and of

covalent charge transfer. Table 2 exemplifies the situation for Al^{3+}. Obviously, on-acceptor hole states leading to Al^{4+} are highly unfavourable. ESR investigations furnished evidence in favour of V_K hole centres (i.e. one hole delocalized over two neighbouring ligands) [32], but there are no such indications for other acceptors in $BaTiO_3$.

Table 2. Hole formations at Al_{Ti}^{3+}. Total embedded-cluster energies are renormalized to the localized off-acceptor π-type hole state. The results include lattice relaxation.

Defect	ΔE_{total}^{UHF} (eV)	ΔE_{total}^{MP2} (eV)	ΔE_{total}^{BLYP} (eV)
Al_{Ti}^{3+}–$O_O^-(\pi)$	0.0	0.0	0.0
Al_{Ti}^{3+}–(deloc.(π))$^-$	+2.5	+0.4	−0.8
Al_{Ti}^{3+}–(deloc.(σ))$^-$	+3.7	+1.9	—
Al_{Ti}^{3+}–($V_K(\pi)$)	+1.0	0.0	−0.4
Al_{Ti}^{3+}–($V_K(\sigma)$)	+2.8	+1.6	—

As expected, HF theory favours localized off-acceptor π-type holes. The next most favoured distribution is the V_K π-type hole one (figure 2), but this is less favourable by 1 eV.

The situation is even worse for completely delocalized states. Again, electron correlation supports hole delocalization. The correlated calculations reported in table 2 confirm that all hole states are of comparable energy. Most favourable are the delocalized state and the formation of V_K centres. However, there is no clear indication in favour of the latter species. But the results suggest a delicate balance between the local electronic structure and defect-induced lattice distortions: increasing the acceptor ionicity would lead to localized off-acceptor holes, whereas a reduced ionicity implies hole delocalization. In an intermediate small 'window', the formation of V_K centres might be the most favourable scenario. This also explains why V_K centres are rarely observed in oxides. Experimentally, the Al cation fits into this window, but also the present embedded-cluster model is close to this situation. Interestingly, V_K centres have been also proposed to occur in Al_2O_3 [33].

Due to reduced bonding, σ-type V_K centres are less favourable by 1.6–1.8 eV than π-type ones. All of the ion displacements are smaller in the σ-type modification. We stress that these results refer to Al^{3+} acceptors, but it is recalled that holes doped into the Cu–O planes of high-T_c oxides are assumed to populate σ-type oxygen orbitals [34]; this population, following our preliminary calculations, is related to the occupation of copper $3d_{x^2-y^2}$ states, and to the presence of strong electron correlations. Our present results assume particular importance, since V_K centres (upon addition of a second hole) bear a resemblance to small intersite hole bipolarons. Thus, we may expect the same relaxation behaviour for hypothetical π-type and σ-type hole bipolarons in high-T_c oxides. Due to moderate lattice distortions, the latter species would be more appropriate for coherent motions. Speculatively, we might suggest that σ-type bipolarons could facilitate superconductivity, thereby supporting the scenario of Alexandrov and Mott [4]. Certainly, our speculations merit further detailed investigations.

We finally review trapped-hole bipolarons in $BaTiO_3$; the details of the calculations are discussed extensively in references [13, 14]. Ti-site Mg^{2+} is considered as the actual acceptor cation. Two geometrical hole–acceptor configurations are compared: the bipolaron with two holes on neighbouring oxygen ions (i.e. literally a V_K centre with one additional hole), and a linear complex, $O^- - Mg_{Ti}^{2+} - O^-$. The presence of two holes introduces a natural driving force towards localization, of which the linear complex corresponds to minimizing

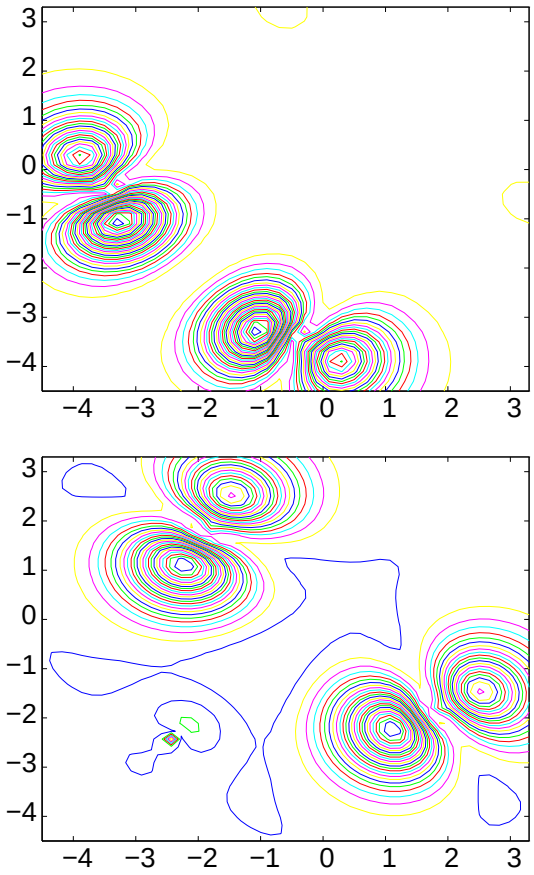

Figure 2. A hole-spin-density plot of π-type (top) and σ-type (bottom) V_K centres trapped at Al_{Ti}^{3+}. The occupation of oxygen 2p orbitals can be clearly seen. The acceptor is at $(x, y) = (0, 0)$ in both cases. All xy-coordinates in the figures are given in atomic units. The interatomic separation between the oxygen partners forming the V_K defect is 2.3 Å and 2.6 Å for localization in π- and σ-type oxygen orbitals, respectively. The perfect-lattice separation is 2.8 Å.

the interhole Coulomb repulsion. The two hole complexes have been studied under different conditions: (1) HF treatment of the cluster employing a rigid and perfectly structured crystal lattice—only the actual O^- partners are allowed to relax; (2) a HF description of the cluster including lattice relaxation; and (3) correlated calculations (MP2 and DFT). To save on required computer capacity, further geometry optimizations have been performed at the DFT level (LSDA and BLYP) only.

We first survey the perfect-lattice HF simulations. Electronic interactions between the O^- ions and nearby crystal ions favour the spin triplet over the singlet state. Due to its antisymmetrical charge distribution, the triplet-state bipolaron benefits most from this interaction. Increasing the bipolaron bond length rapidly disturbs the bipolaron-type states due to hole-state delocalizations. But energetically most favourable is the linear complex. This expected result reflects the fact that delocalized holes are not favoured within the HF theory. The linear configuration with either spin is 1 eV more favourable than the triplet-state bipolaron.

Next we consider the effect of lattice deformations. Most importantly, our ECC demonstrates that defect-induced lattice relaxation and electronic correlations stabilize hole bipolarons in $BaTiO_3$. Lattice relaxations increase the localization of bipolaron states, and favour the spin-singlet state. Thus, such relaxations make possible embedded O_2^{2-} molecules, analogous to isoelectronic F_2 dimers. Noticeably, both species are unstable within the HF theory (e.g. see [14]). The ultimate stability is established by correlation-induced bonding terms. Binding energies of bipolarons can be estimated as the energy difference $E(\mathrm{BP}) - E(\mathrm{O^-}\text{–}\mathrm{Mg}\text{–}\mathrm{O^-})$, since, from shell-model estimates, the competitive linear complex is only weakly bound in $BaTiO_3$. We obtain -0.41 eV (MP2), -1.13 eV (DFT-BLYP), and -2.1 eV (DFT-LSDA). The calculated bond lengths are 1.48 Å (LSDA) and 1.55 Å (BLYP). As is frequently observed [22], LSDA overestimates the degree of bonding. The accurate binding energy is bounded by the BLYP and MP2 values.

We believe that paired holes are of general importance in any oxide. Possible differences will refer to the occupation of π- or σ-type oxygen 2p orbitals giving different bonding strengths. Finally, we emphasize that the singlet–triplet splitting of bipolaron states, i.e. the 'spin gap', depends on the strength of the lattice relaxations. Whereas in perfect lattices the triplet state is preferred, the singlet state becomes the most favourable upon lattice distortion. For π-type bipolarons in $BaTiO_3$, from our MP2 calculations, the spin gap becomes 1.50 eV in this case. We note that this value is essentially intrinsic to the hole bipolarons in $BaTiO_3$, and does not depend on the specific nature of the magnesium acceptor ion. In particular, the bipolaron states are not contaminated by magnesium orbitals; we therefore expect a similar spin gap for the possibly existing isolated bipolarons in $BaTiO_3$. In their bipolaron theory of high-T_c superconductivity, Alexandrov and Mott suggested a spin gap of a few tens of meV [4]. Such a small value would indicate that, compared with the case for $BaTiO_3$, lattice relaxations are present but less developed in high-T_c oxides. This observation is important if coherent motion of bipolarons is to be required.

Acknowledgments

We gratefully acknowledge the financial support of this work by the Deutsche Forschungsgemeinschaft (SFB 225). We also thank Professor O F Schirmer and Professor M Wöhlecke for many valuable discussions.

References

[1] Possenriede E, Jacobs P, Kröse H and Schirmer O F 1992 *Appl. Phys.* A **55** 73
[2] Holtmann L 1989 *Phys. Status Solidi* a **113** K89
[3] Varnhorst T, Schirmer O F, Kröse H, Scharfschwerdt R and Kool T W 1996 *Phys. Rev.* B **53** 116
[4] Alexandrov A S and Mott N F 1994 *Rep. Prog. Phys.* **57** 1197
[5] Anderson P W 1975 *Phys. Rev. Lett.* **34** 953
[6] Schlenker C 1985 *Physics of Disordered Materials: Mott Festschrift* vol 3, ed D Adler, H Fritzsche and S R Ovshinsky (New York: Plenum)
[7] Donnerberg H and Bartram R H 1996 *J. Phys.: Condens. Matter* **8** 1687
[8] Hay W R and Wadt P J 1985 *J. Chem. Phys.* **82** 270
[9] Amos R D *et al* 1994 *Cambridge Analytic Derivatives Package (CADPAC)* version 5.2, Cambridge University
[10] Vosko S H, Wilk L and Nusair M 1980 *Can. J. Phys.* **58** 1200
[11] Becke A D 1988 *Phys. Rev.* A **38** 3098
[12] Lee C, Yang W and Parr R G 1988 *Phys. Rev.* B **37** 785
[13] Donnerberg H and Birkholz A 1995 *J. Phys.: Condens. Matter* **7** 327
[14] Donnerberg H 1995 *J. Phys.: Condens. Matter* **7** L689
[15] Lewis G V and Catlow C R A 1986 *J. Phys. Chem. Solids* **47** 89

[16] Catlow C R A and Mackrodt W C (ed) 1982 *Computer Simulation of Solids (Springer Lecture Notes in Physics 166)* (Berlin: Springer)
[17] Leslie M 1983 *Solid State Ion.* **8** 243
[18] Vail J M, Harker A H, Harding J H and Saul P 1984 *J. Phys. C: Solid State Phys.* **17** 3401
[19] Kunz A B and Klein D L 1978 *Phys. Rev.* B **17** 4614
[20] Bar'yudin L É 1991 *Sov. Phys.–Solid State* **33** 1820
[21] Vail J M 1990 *J. Phys. Chem. Solids* **51** 589
[22] Fulde P 1991 *Electron Correlations in Molecules and Solids (Springer Series in Solid-State Sciences 100)* (Berlin: Springer)
[23] Szabo A and Ostlund N S 1989 *Modern Quantum Chemistry—Introduction to Advanced Electronic Structure Theory* (New York: McGraw-Hill)
[24] Umrigar C J, Filippi C and Gonze X 1996 Generalized gradient approximations to density functional theory: comparison with exact results *Recent Developments and Applications of Density Functional Theory* ed J M Seminario (Amsterdam: Elsevier)
[25] Handy N C 1994 Density functional theory *Lecture Notes in Chemistry (Springer Lecture Notes in Quantum Chemistry II)* vol 64, ed B O Roos (Berlin: Springer)
[26] Shluger A L, Kotomin E A and Kantorovich L N 1986 *J. Phys. C: Solid State Phys.* **19** 4183
[27] Shluger A L, Heifets E N, Gale J D and Catlow C R A 1992 *J. Phys.: Condens. Matter* **4** 5711
[28] Meng J, Jena P and Vail J M 1990 *J. Phys.: Condens. Matter* **2** 10 371
[29] Izen E H, Mazo R M and Kemp J C 1973 *J. Phys. Chem. Solids* **34** 1431
[30] Haldane F D M and Anderson P W 1976 *Phys. Rev.* B **13** 2553
[31] Stoneham A M and Sangster M J L 1981 *Phil. Mag.* B **43** 609
[32] Possenriede E, Jacobs P and Schirmer O F 1992 *J. Phys.: Condens. Matter* **4** 4719
[33] Kantorovich L, Stashans A, Kotomin E and Jacobs P W M 1994 *Int. J. Quantum Chem.* **52** 1177
[34] Fink J, Nücker N, Romberg H A and Fuggle J C 1989 *IBM J. Res. Dev.* **33** 372